Supporting Information for

High-Performance Anthracene-Linked Covalent Triazine Framework with Dual Functions for CO_2 Capture and Supercapacitor Applications

Ming-Chieh Lin,[a] Shiao-Wei Kuo[a,b]* and Mohamed Gamal Mohamed[a,c,*]

[a]Department of Materials and Optoelectronic Science, College of Semiconductor and Advanced Technology Research, Center for Functional Polymers and Supramolecular Materials, National Sun Yat-Sen University, Kaohsiung 804, Taiwan.

[b]Department of Medicinal and Applied Chemistry, Kaohsiung Medical University, Kaohsiung 807, Taiwan.

[c]Chemistry Department, Faculty of Science, Assiut University, Assiut 71516, Egypt.

Corresponding authors:

E-mail: (kuosw@faculty.nsysu.edu.tw (S. W. Kuo) and mgamal.eldin12@yahoo.com and mgamal.eldin12@aun.edu.eg (M. G. Mohamed).

Characterization

FTIR spectra were collected on a Bruker Tensor 27 FTIR spectrophotometer with a resolution of 4 cm^{-1} by using the KBr disk method. The thermal stabilities of the samples were performed by using a TG Q-50 thermogravimetric analyzer under an N_2 atmosphere; the cured sample (ca. 5 mg) was put in a Pt cell with a heating rate of 20 °C min^{-1} from 100 to 800 °C under a N_2 flow rate of 60 mL min^{-1}. Wide-angle X-ray diffraction (WAXD) patterns were measured by the wiggler beamline BL17A1 of the National Synchrotron Radiation Research Center (NSRRC), Taiwan. A triangular bent Si (111) single crystal was used to get a monochromated beam having a wavelength (λ) of 1.33 Å. The morphologies of the polymer samples were examined by Field emission scanning electron microscopy (FE-SEM; JEOL JSM7610F) and also by transmission electron microscope (TEM) using a JEOL-2100 instrument at an accelerating voltage of 200 kV. BET surface area and porosimetry measurements of samples (ca. 40–100 mg) were measured using BEL Master™/BEL sim™ (v. 3.0.0). N_2 adsorption and desorption isotherms were generated through incremental exposure to ultrahigh-purity N_2 (up to ca. 1 atm) in a liquid N_2 (77 K) bath. Surface parameters were calculated using BET adsorption models in the instrument's software. The pore size of the prepared samples was determined by using nonlocal density functional theory (NLDFT).

Electrochemical Analysis

Working Electrode Cleaning: Before use, the glassy carbon electrode (GCE) was polished several times with 0.05-µm alumina powder, washed with EtOH after each polishing step, cleaned through sonication (5 min) in a water bath, washed with EtOH, and then dried in air.

Electrochemical Characterization

The electrochemical experiments were performed in a three-electrode cell using an Autolab potentiostat (PGSTAT204) and 1 M KOH as the aqueous electrolyte. The GCE was used as the working electrode (diameter: 5.61 mm; 0.2475 cm^2); a Pt wire was used as the counter electrode; Hg/HgO (RE-1B, BAS) was the reference electrode. All reported potentials refer to the Hg/HgO potential. A slurry was prepared by dispersing ANT-CTFs (2 mg), carbon black (2 mg), and Nafion (10 wt %) in a mixture of (EtOH/ H_2O) (200 μL: 800 μL) and then sonicating for 1 h. A portion of this slurry (10 μL) was pipetted onto the tip of the electrode, which was then dried in air for 30 min before use. The electrochemical performance was studied through CV at various sweep rates (5–200 mV s^{-1}) and through the GCD method in the potential range from -1.0 V and 0.0 V (vs. Hg/HgO) at various current densities (0.5–20 A g^{-1}) in 1 M KOH as the aqueous electrolyte solution.

The specific capacitance was calculated from the GCD data using the equation.

$$C_s = (I\Delta t)/(m\Delta V) \qquad (1)$$

Where C_s (F g^{-1}) is the specific capacitance of the supercapacitor, I (A) is the discharge current, ΔV (V) is the potential window, Δt (s) is the discharge time, and m (g) is the mass of the NPC on the electrode. The energy density (E, W h kg^{-1}) and power density (P, W kg^{-1}) were calculated using the equations.

$$E = 1000C(\Delta V)^2/(2 \times 3600) \qquad (2)$$

$$P = E/(t/3600) \qquad (3)$$

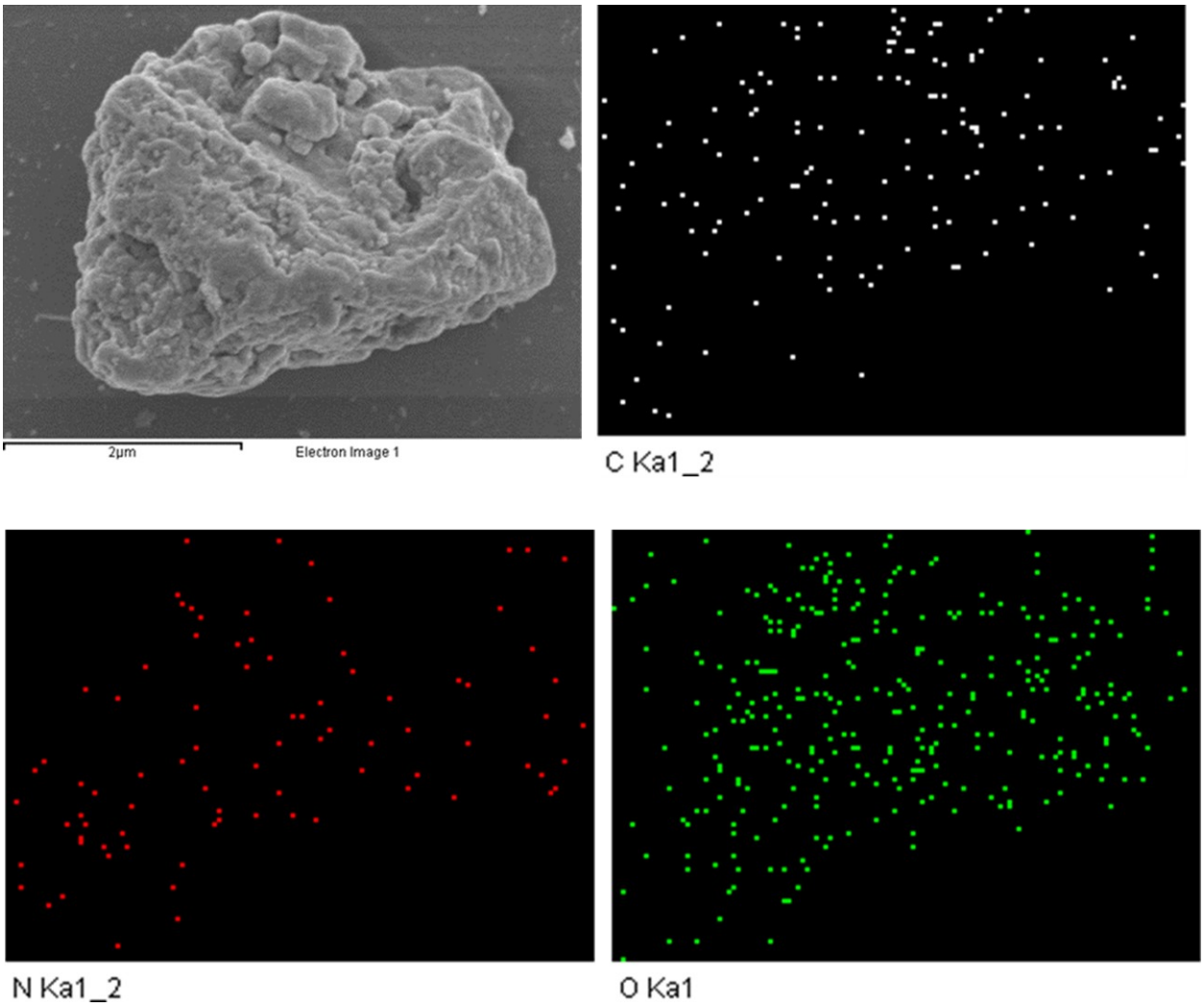

Figure S1. SEM-EDS elemental mapping analysis of ANT-CTF-10-500.

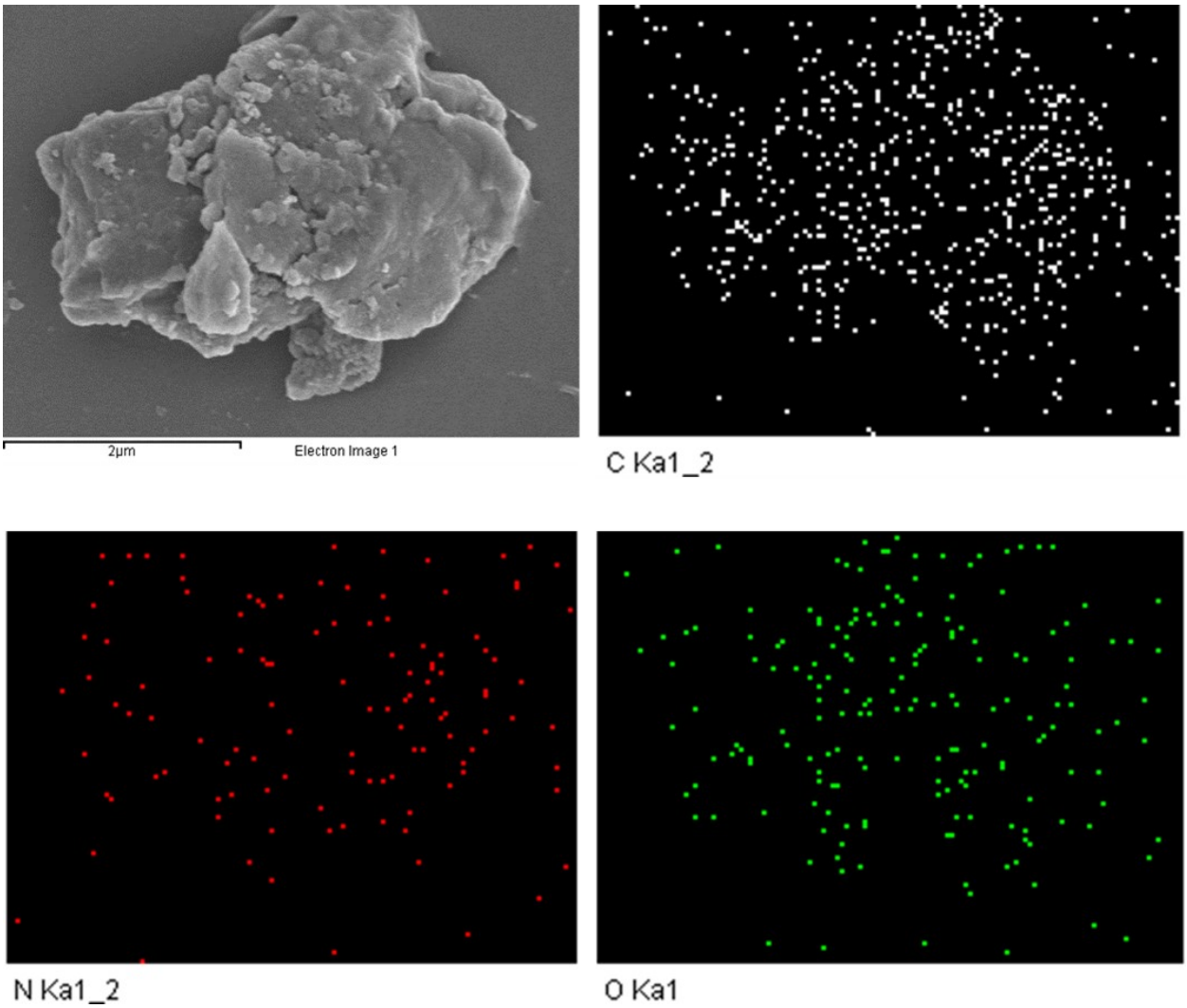

Figure S2. SEM-EDS elemental mapping analysis of ANT-CTF-20-500.

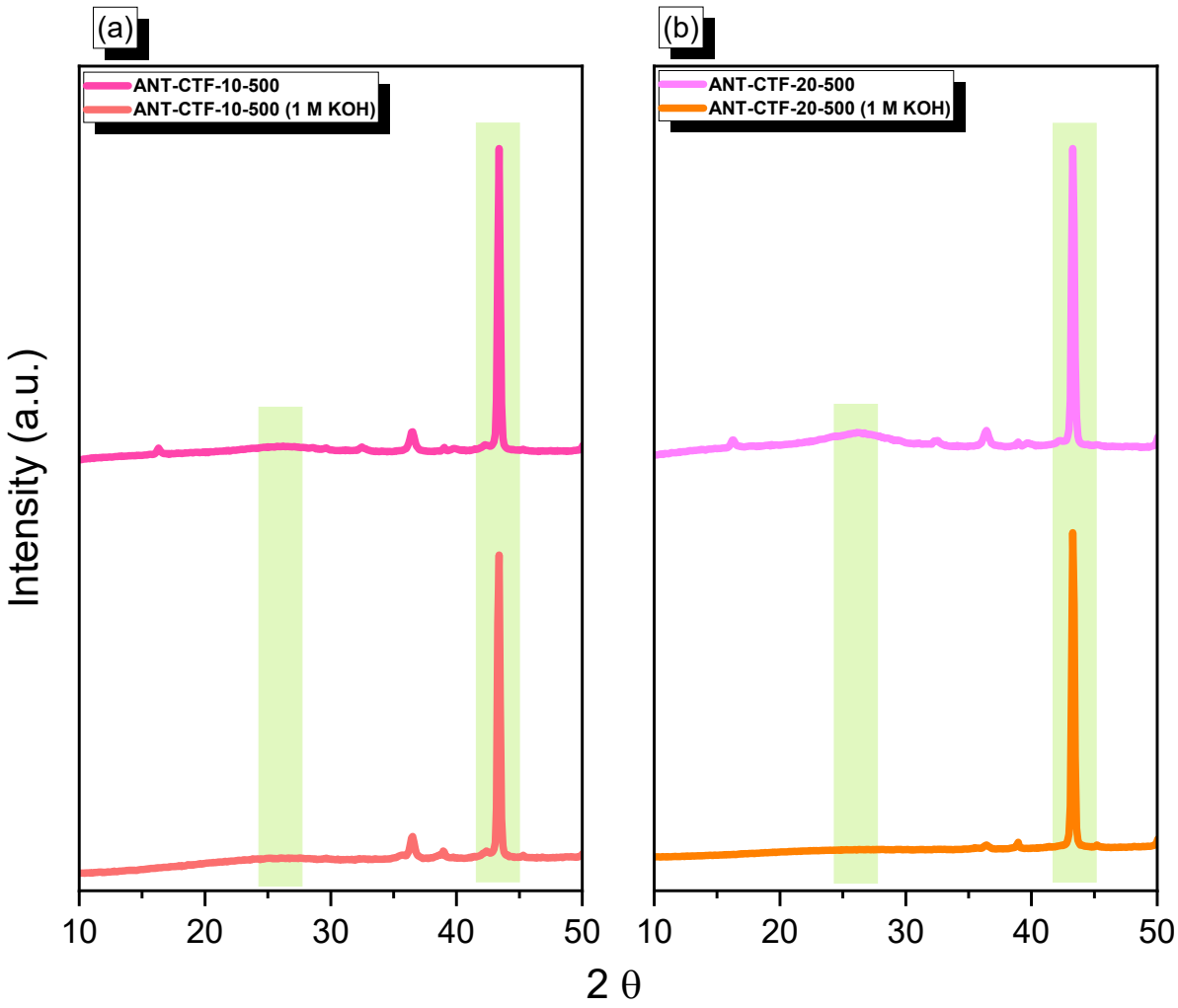

Figure S3. XRD data of (a) ANT-CTF-10-500 and (b) ANT-CTF-20-500 immersion in KOH solution (1 M).

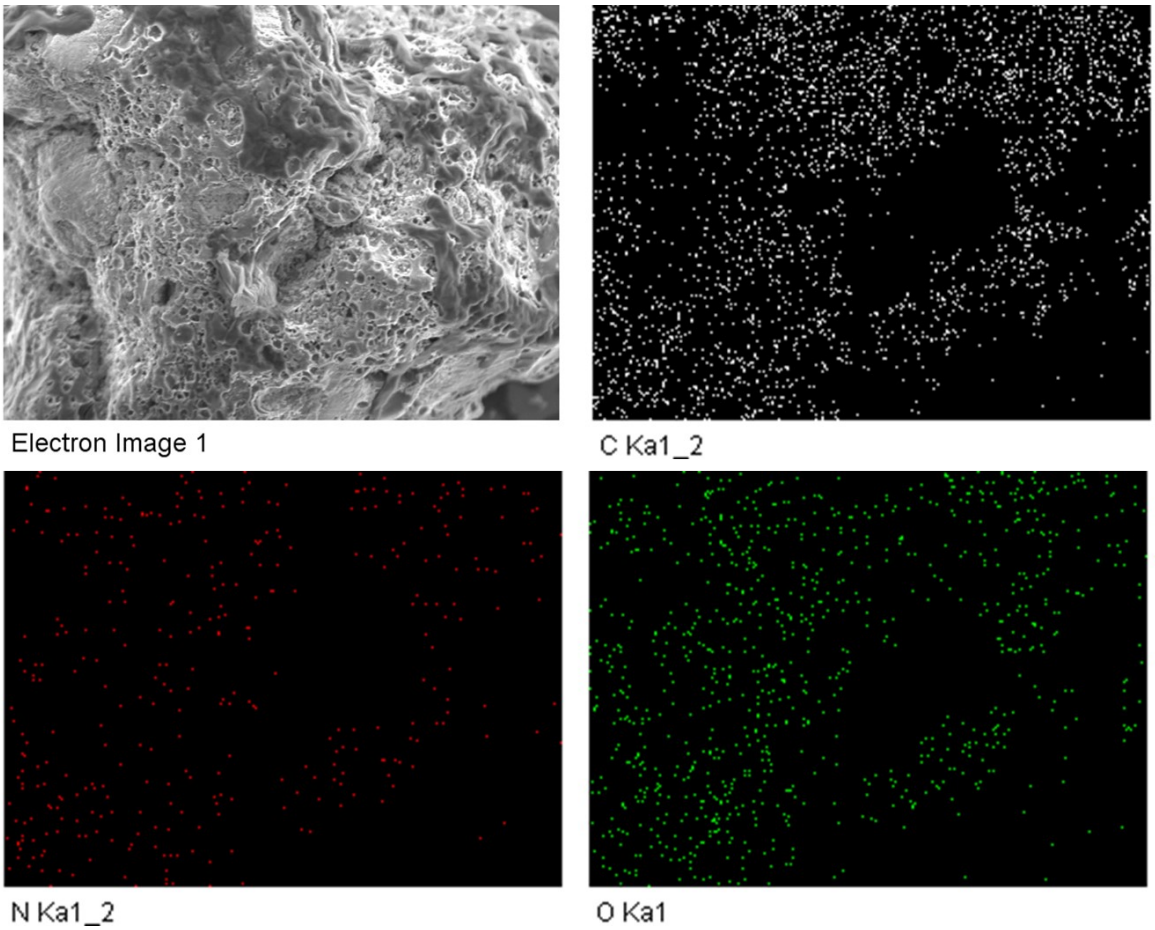

Figure S4. SEM-EDS elemental mapping analysis of ANT-CTF-10-500 after immersion in KOH solution (1 M).

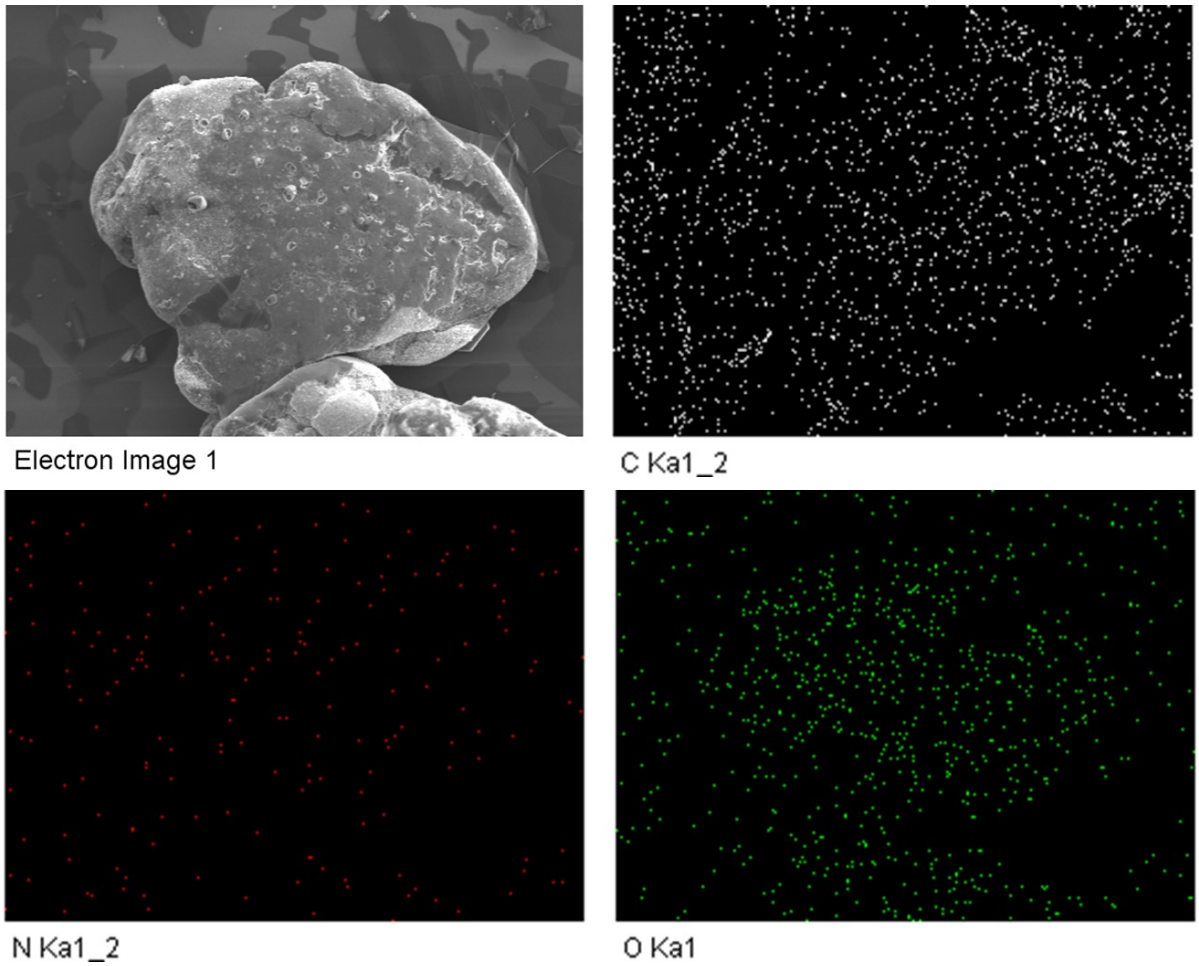

Figure S5. SEM-EDS elemental mapping analysis of ANT-CTF-20-500 after immersion in KOH solution (1 M).

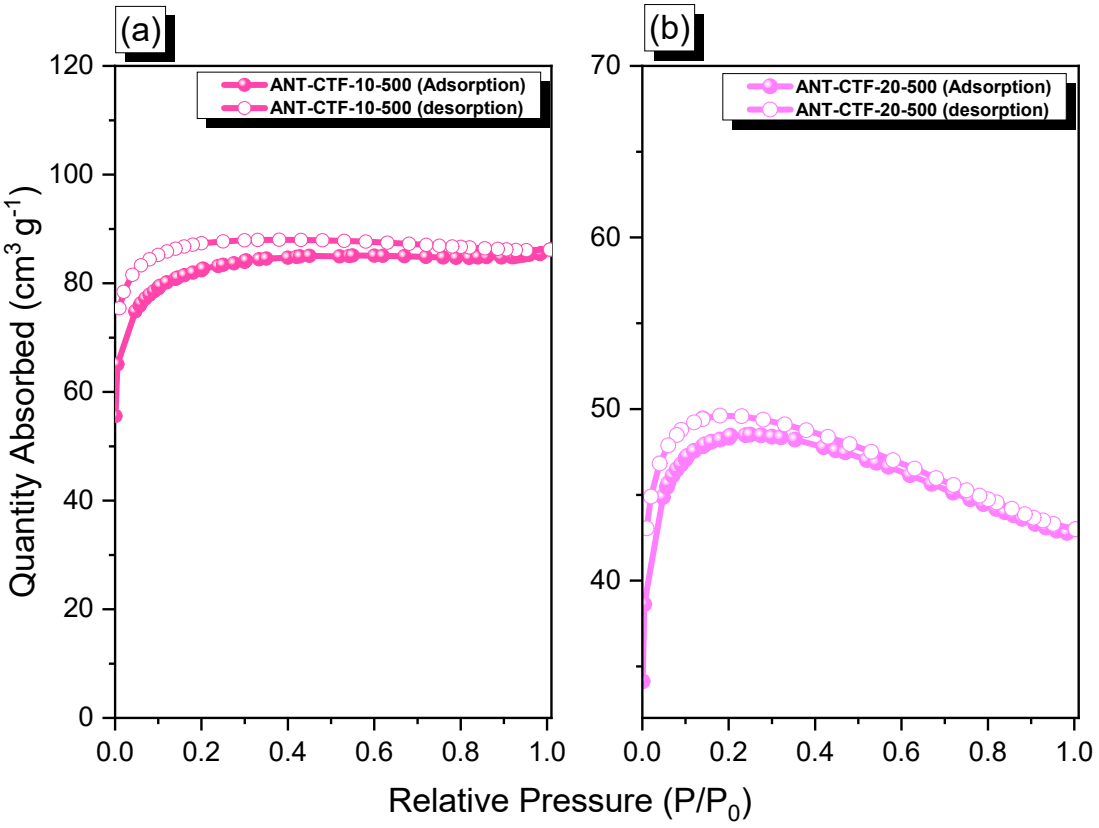

Figure S6. BET analysis of (a) ANT-CTF-10-500 and (b) ANT-CTF-20-500 after immersion in KOH solution (1 M).

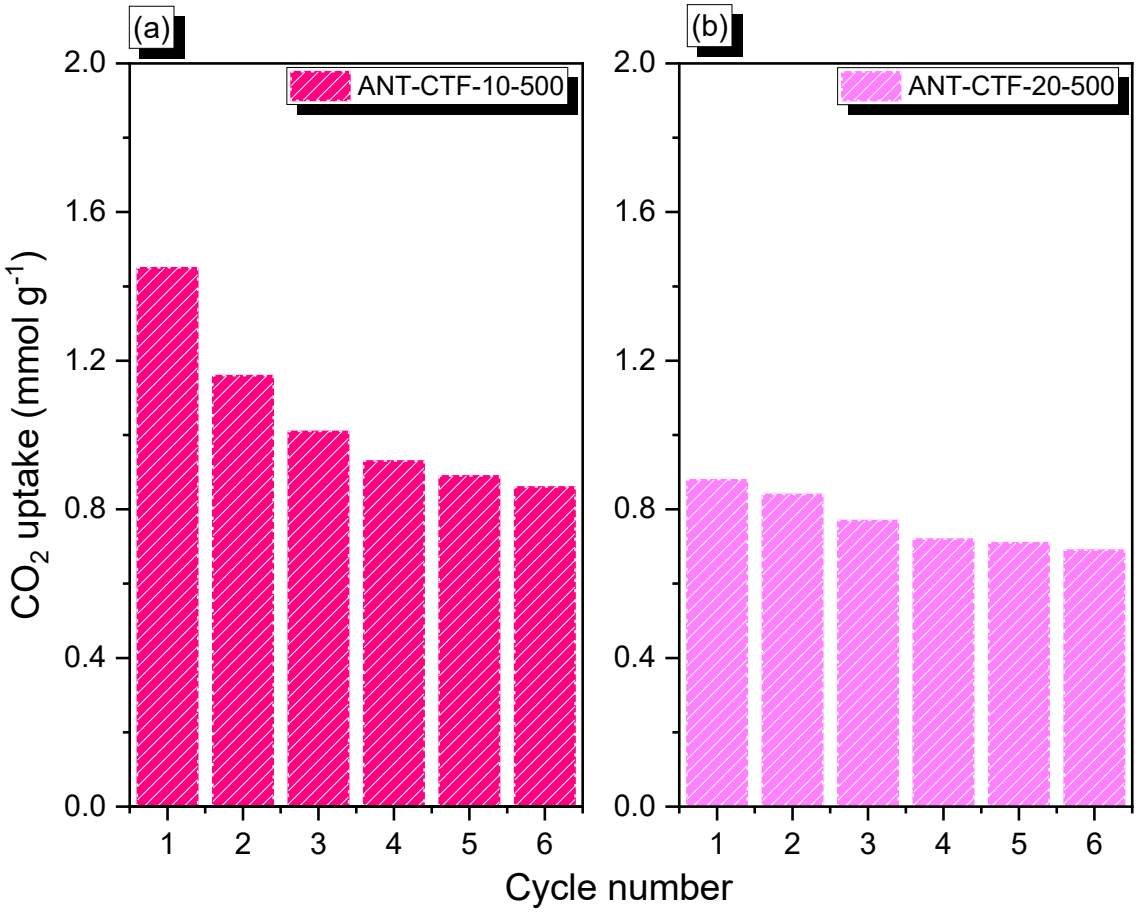

Figure S7. CO_2 uptake of (a) ANT-CTF-10-500 and (b) ANT-CTF-20-500 after six measurement cycles at 25 °C.

Table S1. TGA data of ANT-6CN and ANT-CTFs.

Sample	T_{d5} (°C)	T_{d10} (°C)	Char yield (%)
ANT-6CN	**200**	**234**	**62**
ANT-CTF-10-500	**353**	**588**	**77**
ANT-CTF-20-500	**492**	**630**	**81**

Table S2. XPS data of N1s and O1S orbitals of synthesized ANT-CTFs.

Sample	N Species			O Species		
	N-6	N-5	N-Q	C-O	C-OH	H_2O
ANT-CTF-10-500	**57.28**	**27.19**	**15.53**	**84.40**	**15.60**	**0.00**
ANT-CTF-20-500	**29.85**	**52.22**	**17.93**	**85.03**	**7.70**	**7.27**

Table S3. Comparison of ANT-CTF-10-500 and ANT-CTF-20-500 for CO_2 uptake with other porous materials.

Sample	CO_2 uptake (mmol/g)	Ref.
ANT-CTF-10-500	**2.14 (at 273 K)**	**This work**
ANT-CTF-10-500	**1.45 (at 298 K)**	**This work**
ANT-CTF-20-500	**1.29 (at 273 K)**	**This work**
ANT-CTF-20-500	**0.88 (at 298 K)**	**This work**
An-CTF-10-500	2.69 (298 K)	S1
An-CTF-20-500	2.63 (298 K)	S1
An-CTF-20-400	2.31(298 K)	S1
An-CTF-10-400	2 (298 K)	S1
FEC-Mel POP	1.34 (298 K)	S2
FEC-PBDT POP	0.51 (298 K)	S2
RIO-13	0.568 (298 K)	S3
RIO-12	0.368 (298 K)	S3
RIO-11m	0.227 (298 K)	S3
RIO-11	0.136 (298 K)	S3
CTF-5-400	1.52 (298 K)	S4
CTF-5-400	2.25 (273 K)	S4
CTF-10-400	1.68 (298 K)	S4
CTF-10-400	2.9 (273 K)	S4

Table S4. Comparison of ANT-CTF-10-500 and ANT-CTF-20-500 for the isosteric adsorption heats (Q_{st}) with other porous materials.

Sample	Q_{st} for CO_2 kJ mol^{-1}	Ref.
ANT-CTF-10-500	**27**	**This work**
ANT-CTF-20-500	**19**	**This work**
cCTF-400	49	S5
cCTF-450	46	S5
cCTF-500	43	S5
CTF-CSU38	39.25	S6
CTF-CSU39	41.3	S6
CTF-CSU40	38.5	S6
CTF-CSU41	44.6	S6
CTF-5-400	26	S4
CTF-10-400	28	S4
CTF-20-400	22	S4
CTF-5-500	26	S4
CTF-10-500	26	S4
CTF-20-500	25	S4
Py-CTF-400	25.9	S7
Py-CTF-500	23.1	S7
TPPy-CTF-400	24.5	S7
TPPy-CTF-500	22.2	S7

References

[S1] M. G. Mohamed, S. U. Sharma, N. Y. Liu, T. H. Mansoure, M. M. Samy, S. V. Chaganti, Y. L. Chang, J. T. Lee and S. W. Kuo. Ultrastable Covalent Triazine Organic Framework Based on Anthracene Moiety as Platform for High-Performance Carbon Dioxide Adsorption and Supercapacitors. *Int. J. Mol. Sci*. 2022, **23**, 3174. doi.org/10.3390/ijms23063174.

[S2] A. O. Mousa, C. H. Chuang, S.W Kuo and M. G. Mohamed. Strategic Design and Synthesis

of Ferrocene Linked Porous Organic Frameworks toward Tunable CO_2 Capture and Energy Storage. *Int. J. Mol. Sci*. 2023, **24**, 12371. doi.org/10.3390/ijms241512371.

[S3] R. A. Maia, F. L. Oliveira, V. Ritleng, Q. Wang, B. Louis and P. M. Esteves. CO_2 Capture by Hydroxylated Azine-Based Covalent Organic Frameworks. *Chem. Eur. J*. 2021, **27**, 8048-8055. doi.org/10.1002/chem.202100478.

[S4] G. Wang, K. Leus, S. Zhao and P. V. D. Voort. Newly Designed Covalent Triazine Framework Based on Novel N-Heteroaromatic Building Blocks for Efficient CO_2 and H_2 Capture and Storage. *ACS Appl. Mater. Interfaces* 2018, **10**, 1, 1244–1249. DOI: doi.org/10.1021/acsami.7b16239.

[S5] Y. J. Lee and S. N. Naidu and A. Coskun. Chemically activated covalent triazine frameworks with enhanced textural properties for high capacity gas storage. *ACS Appl. Mater. Interfaces* 2017, **9**, 30679–30685. doi.org/10.1021/acsami.7b08930.

[S6] Y. Fu, Z. Wang, S. Li, X. He, C. Pan, J. Yan and G. Yu. Functionalized Covalent Triazine Frameworks for Effective CO_2 and SO_2 Removal. *ACS Appl. Mater. Interfaces* 2018, **10**, 42, 36002–36009. DOI: doi.org/10.1021/acsami.8b13417

[S7] Y. Chen, X. Hu, J. Guo, Z. Guo, H. Zhan and S. Du. Optimizing CO_2 capture and separation in pyrene derived covalent triazine frameworks. *Eur. Polym. J*. 2022, **171**, 111–215. doi.org/10.1016/j.eurpolymj.2022.111215.